Holographic complexity and phase transition for AdS black holes

Hong-Yue Jiang[1,2] Meng-Ting Wang[1,2] and Yu-Xiao Liu[1,2,*]

[1]*Lanzhou Center for Theoretical Physics, Key Laboratory of Theoretical Physics of Gansu Province,*
Key Laboratory for Quantum Theory and Applications of the Ministry of Education,
Lanzhou University, Lanzhou, Gansu 730000, China
[2]*Institute of Theoretical Physics and Research Center of Gravitation,*
School of Physics Science and Technology, Lanzhou University,
Lanzhou 730000, China

Recently, the complexity equals any gravitational observable conjecture has been proposed in [Phys. Rev. Lett. **128**, 081602 (2022)], which is an extension of the complexity equals volume proposal. These gravitational observables are referred to as generalized volumes. In this paper, we investigate the generalized volume complexity for black holes with one or two horizons respectively. We verify that the turning time is universal and independent of the Cauchy horizon. Not only does this phase transition occur once, but it may also occur two or more times depending on the number and height of the effective potential peaks. On the other hand, we confirm that the generalized volume complexity can be divided based on the shape of the effective potential. We then discuss the nonsmooth transition from the Reissner–Nordström–anti-de Sitter (AdS) black hole to the Schwarzschild-AdS black hole.

I. INTRODUCTION

In the last three decades, the holographic principle has attracted widespread attention [1–48]. In 1997, Maldacena made the first concrete realization of the holographic principle [1]. The calculation shows that the conformal field theory (CFT) of d-dimensional spacetime is equivalent to the quantum gravity theory in $(d + 1)$-dimensional asymptotic anti-de Sitter (AdS) spacetime, known as the AdS/CFT correspondence [1,2]. After 26 years of development, the AdS/CFT correspondence has become a popular and important research direction in quantum gravity and quantum information.

On the other hand, Susskind and Maldacena proposed a new idea regarding the holographic principle [3]. They observed the similarities between the Einstein-Podolsky-Rosen (EPR) paradox and the Einstein-Rosen (ER) bridge and referred to this as the ER = EPR relation [3,4]. According to ER = EPR, two systems are connected by an ER bridge if and only if they are entangled. The ER bridge is not a static object, it grows linearly with time for a very long time. However, for a black hole system, the dual system reaches thermal equilibrium quickly. Therefore, entanglement entropy is not enough. For a complete description of the growth of the ER bridge, Susskind introduced quantum computational complexity as a measure of the volume growth of the ER bridge [5].

Complexity quantifies the level of difficulty associated with performing a task using a set of simple operations. In quantum complexity, a quantum circuit is constructed by combining simple gates that act on a few qubits to perform a particular operation using a unitary operator. In the context of black holes and holography, quantum complexity has recently triggered significant interest, offering a new perspective in the ongoing effort to connect quantum information theory with quantum gravity. In recent years, there has been dramatic progress toward holographic complexity [15–37], circuit complexity in quantum field theory [49–53], Krylov complexity [54–61], and complexity in de Sitter space [62,63].

Under the framework of AdS/CFT, there are three important proposals regarding the holographic complexity: complexity equals volume (CV) [5–7], complexity equals action (CA) [10,11], and complexity equals spacetime volume (CV 2.0) [12]. The CV proposal maintains that complexity is determined by the maximal volume slice of a hypersurface anchored on the CFT boundary, i.e.,

$$\mathcal{C}_V = \max_{\partial\Sigma}\left[\frac{V(\Sigma)}{G_N L}\right], \quad (1.1)$$

where Σ is a hypersurface anchored on the boundary CFT slice, G_N denotes Newton's constant in the bulk gravitational theory, and L is a constant with length dimension which often replaced by AdS radius. Based on the CV proposal, Stanford and Susskind calculated the maximum volume hypersurface inside the AdS black hole after it is disturbed by shock wave geometries and proposed the butterfly effect of complexity [6]. Recently, an analytical expression about the butterfly effect of complexity for an inverted harmonic oscillator was obtained in Refs. [13,14]. For the CA proposal, complexity is defined as the action of the Wheeler–de Witt patch, which is given by

$$\mathcal{C}_A = \frac{I_{\mathrm{WdW}}}{\pi\hbar}, \qquad (1.2)$$

where the Wheeler–de Witt patch is the set of all spacelike hypersurfaces in spacetime [15]. And the CV 2.0 proposal is optimized based on the first two conjectures. In this case, complexity equals the volume of the Wheeler–de Witt patch, that is,

$$\mathcal{C}_{SV} = \frac{V_{\mathrm{WdW}}}{G_N L^2}. \qquad (1.3)$$

Among them, all of holographic complexity proposals have ambiguous definitions, just like the ill-defined constant L in the CV or CV 2.0 proposal, or a similarly indeterminate length scale that occurs on the null boundaries of the Wheeler–de Witt patch. In this regard, some scholars believe that this ambiguity is not a shortcoming of the theory itself but a feature of holographic complexity because there are similar ambiguities in quantum computational complexity, such as the choice of a quantum gate set. The concept of holographic complexity is generalized in Refs. [33–35]. The authors defined the new gravitational observable as the generalized volume complexity, i.e.,

$$\mathcal{O}_{F_1, \Sigma_{F_2}}(\Sigma_{\mathrm{CFT}}) = \frac{1}{G_N L} \int_{\Sigma_{F_2}} d^d\sigma \sqrt{h} F_1(g_{\mu\nu}; X^\mu), \qquad (1.4)$$

where Σ_{F_2} is an codimension-1 hypersurface anchored on the CFT slice Σ_{CFT}, h is the induced metric on the Σ_{F_2}, and both F_1 and F_2 are scalar functions of the bulk metric $g_{\mu\nu}$ and of an embedding coordinate X^μ of the Σ_{F_2}. If the CFT slice is a constant time slice in the boundary CFT, Σ_{CFT} can be rewritten as Σ_τ; i.e., $\partial\Sigma_{F_2} = \Sigma_\tau$. Σ_{F_2} is determined by

$$\delta_X \left(\int_{\Sigma_{F_2}} d^d\sigma \sqrt{h} F_2(g_{\mu\nu}; X^\mu) \right) = 0. \qquad (1.5)$$

In the general case, there is no correlation between F_1 and F_2. However, for $F_1 = F_2 = 1$, the extremal hypersurface obtained by Eq. (1.5) is the extremal volume slice in the CV proposal (1.1). Extending this example, they analyzed in

detail the case where $F_1 = a_1(r)$, $F_2 = a_2(r)$, and the conjecture that "complexity equals anything" is validated across multiple models [36].

In our previous work [37], we considered the generalized volume complexity for the four-dimensional Reissner-Nordström-AdS (RN-AdS) black hole, whose growth rates exhibit a discontinues change at a certain boundary time. This discontinuous change in bulk belongs to a phase transition, and the transition time is defined as a turning time. However, our analysis of the RN-AdS black hole still has certain limitations. First, It is possible that the existence of the turning time is universal and not unique. Therefore, we need to consider more models to get a more general law. Second, we believe that the impact of the disappearance of the Cauchy horizon on the growth rate of the generalized volume complexity for black holes with two horizons at late time also deserves discussion. Finally, all the above calculations in Ref. [37] were done for the case of $F_1 = F_2$. We believe that these questions are also worth exploring for the more general case of $F_1 \neq F_2$.

In this paper, we would like to investigate the generalized volume complexity for the planar AdS black hole, the charged Bañados-Teitelboim-Zanelli (BTZ) black hole, and the five-dimensional Gauss-Bonnet-AdS black hole with some different gravitational observables and additionally discuss the difference between the RN-AdS black hole at the limit of $Q \to 0$ and $Q = 0$. Our findings reveal that the Cauchy horizon is not a necessary condition for the existence of turning time. When we choose a suitable gravitational observable, we can always find such a phase transition, whether or not the Cauchy horizon exists. Furthermore, there may not be only one turning time but rather two or even more, depending on the properties of the effective potential. On the other hand, we will demonstrate that the generalized volume complexity can be divided into two categories according to the properties of the effective potential at the singularity or the Cauchy horizon, resulting in different parameter spaces of coupling constants. During a supplementary discussion of the RN-AdS black hole, we find that with $Q \to 0$ the generalized volume complexity does not smoothly transform into to the AdS-Schwarzschild solution case. In addition, we find that for the more general case of $F_1 \neq F_2$ the existence of the turning time is still universal. Different from the $F_1 = F_2$ case, in this situation, the existence of the turning time depends not only on the number of the effective potential peaks decreasing from left to right but also on the form of F_1. Regarding the growth rate of the generalized volume complexity, its linear growth in the late-time limit can still be satisfied, although the early evolution is not necessarily monotonic.

In Sec. II, we review the generalized volume complexity using the planar AdS black hole as an example. In Sec. III, we analyze the generalized volume complexity of the black holes with a single horizon. Taking the planar AdS black hole and the five-dimensional Gauss-Bonnet-AdS black hole as

examples, we find that the turning time is independent of the limit of the Cauchy horizon and divide the generalized volume complexity into two categories based on the shape of the effective potential. In Sec. IV, we analyze the generalized volume complexity of the black hole with two horizons. Taking the charged BTZ black holes as an example, we examine the generalized volume complexity constructed by spacetime curvature or matter content respectively. In addition, we discuss the unsmooth transition of the RN-AdS black hole to the AdS-Schwarzschild black hole. In Sec. V, we calculate the generalized volume complexity and turning time for the $F_1 \neq F_2$ case and explain how it differs from the case of $F_1 = F_2$. Finally, the discussion and conclusion are given in Sec. VI.

II. COMPLEXITY EQUALS ANYTHING CONJECTURE

In this section, we review the "complexity equals anything" conjecture using the planar AdS black hole as an example, presented in Ref. [33]. The metric of the $(d+1)$-dimensional eternal AdS planar black hole can be described in Eddington-Finkelstein coordinates,

$$ds^2 = -f(r)dv^2 + 2dvdr + \frac{r^2}{L^2}d\vec{x}^2, \qquad (2.1)$$

where $f(r) = \frac{r^2}{L^2}\left(1 - \frac{r_h^d}{r^d}\right)$ and $v = t + r_*(r)$ with $r_*(r) = -\int_r^\infty \frac{dr'}{f(r')}$. This geometry is regarded as the dual of two decoupled CFTs on planar spatial slices Σ, which are entangled in the thermofield double (TFD) state

$$|\psi_{\text{TFD}}(\tau)\rangle = \sum_n e^{-\beta E_n/2 - iE_n\tau}|n\rangle_{\text{L}} \otimes |n\rangle_{\text{R}}, \qquad (2.2)$$

where β is the inverse of the temperature, E_n is the energy eigenstate, and L and R symbolize the two entangled sides of the planar AdS black hole and label the quantum states $|n\rangle_L$ and $|n\rangle_R$, respectively. The time τ is associated with the left and right boundaries with $t_L = t_R = \tau/2$. According to Ref. [33], when we select $F_1 = F_2 = a(r)$, the general expression of complexity can be obtained by

$$\mathcal{C} = \max_{\partial\Sigma=\Sigma_\tau}\left[\frac{1}{G_NL}\int_\Sigma d^d\sigma\sqrt{h}a(r)\right], \qquad (2.3)$$

where σ is a radial coordinate on the hypersurface Σ. Thanks to the planar symmetric, we can parametrize Eq. (2.3) as

$$\mathcal{C} = \frac{V_{d-1}}{G_NL}\int_\Sigma d\sigma\left(\frac{r}{L}\right)^{d-1}\sqrt{-f(r)\dot{v}^2 + 2\dot{v}\,\dot{r}}\,a(r)$$
$$\equiv \frac{V_{d-1}}{G_NL}\int_\Sigma d\sigma\mathcal{L}(r,\dot{v},\dot{r}), \qquad (2.4)$$

where V_{d-1} denotes the volume element of the spatial directions $\vec{x}$. We can refer to $\mathcal{C}$ as the generalized volume complexity and treat the integrand as the Lagrangian $\mathcal{L}$. Choosing the gauge as

$$\sqrt{-f(r)\dot{v}^2 + 2\dot{v}\,\dot{r}} = a(r)\left(\frac{r}{L}\right)^{d-1}, \qquad (2.5)$$

we can note that the $\mathcal{L}$ does not depend explicitly on v, so we can define a conserved momentum P_v:

$$P_v = \frac{a(r)(r/L)^{d-1}(\dot{r} - f(r)\dot{v})}{\sqrt{-f(r)\dot{v}^2 + 2\dot{v}\,\dot{r}}} = \dot{r} - f(r)\dot{v}. \qquad (2.6)$$

According to Eqs. (2.5) and (2.6), we can obtain the extremality conditions

$$\dot{r} = \pm\sqrt{P_v^2 + f(r)a^2(r)\left(\frac{r}{L}\right)^{2(d-1)}}, \qquad (2.7)$$

$$\dot{v} = \frac{1}{f(r)}\left(-P_v \pm \sqrt{P_v^2 + f(r)a^2(r)\left(\frac{r}{L}\right)^{2(d-1)}}\right). \qquad (2.8)$$

Therefore, we can explain this problem as the motion of a classical particle in a potential

$$\dot{r}^2 + U(r) = P_v^2, \qquad (2.9)$$

where the effect potential $U(r)$ is given by

$$U(r) = -f(r)a^2(r)\left(\frac{r}{L}\right)^{2(d-1)}. \qquad (2.10)$$

Based on Eq. (2.5), we can rewrite Eq. (2.4) as

$$\mathcal{C} = \frac{V_{d-1}}{G_NL}\int_\Sigma \frac{a^2(r)(\frac{r}{L})^{2(d-1)}}{\dot{r}}dr. \qquad (2.11)$$

Using Eq. (2.9), we can get $\dot{r} = \pm\sqrt{P_v^2 - U(r)}$. On the other hand, we have $U(r_{\min}) = P_v^2$, where $r_{\min}$ is the minimum radius for the largest generalized volume slice as shown in Fig. 1. Therefore, $\dot{r} = \sqrt{U(r_{\min}) - U(r)}$, and we have

$$\mathcal{C} = \frac{2V_{d-1}}{G_NL}\int_{r_{\min}}^{r_\infty} \frac{a^2(r)(\frac{r}{L})^{2(d-1)}}{\sqrt{P_v^2 - U(r)}}dr$$
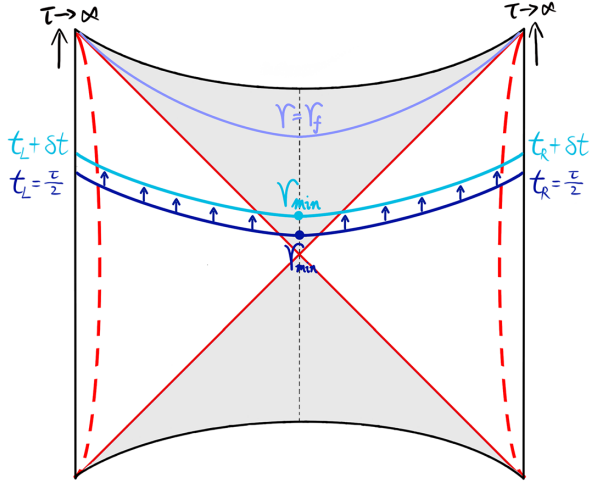$$= -\frac{2V_{d-1}}{G_NL}\int_{r_{\min}}^{r_\infty} \frac{U(r)}{f(r)\sqrt{U(r_{\min}) - U(r)}}dr. \qquad (2.12)$$

FIG. 1. The Penrose diagram of the eternal AdS black hole. The curves are the extremal hypersurfaces anchored at $t_L = t_R = \tau/2$. On the black dashed line $t = 0$, we have $\dot{r}|_{r=r_{\min}} = 0$. When we anchor the boundary time as $\tau \to \infty$, the extremal hypersurface becomes a constant-r slice, i.e., $r = r_f$. This image refers to Fig. 1 in Ref. [33].

On the other hand, according to the ingoing coordinates, we can have

$$
\frac{\tau}{2} + r_*(r_\infty) - r_*(r_{\min})
$$
$$
= \int_{v_{\min}}^{v_\infty} dv = \int_{r_{\min}}^{r_\infty} \frac{\dot{v}}{\dot{r}} dr
$$
$$
= \int_{r_{\min}}^{r_\infty} dr \left[\frac{1}{f(r)} - \frac{P_v}{f(r)\sqrt{P_v^2 + f(r)a^2(r)(\frac{r}{L})^{2(d-1)}}} \right].
$$
$$(2.13)$$

We hope to extract the part containing Eq. (2.13) from Eq. (2.12). By following the method provided in Ref. [16], we can rewrite Eq. (2.12) as follows:

$$
\mathcal{C} = \frac{2V_{d-1}}{G_N L} \int_{r_{\min}}^{r_\infty} dr \left[-\frac{P_v^2}{f(r)\sqrt{P_v^2 + f(r)a^2(r)(\frac{r}{L})^{2(d-1)}}} \right.
$$
$$
\left. + \frac{\sqrt{P_v^2 + f(r)a^2(r)(\frac{r}{L})^{2(d-1)}}}{f(r)} + \frac{P_v}{f(r)} - \frac{P_v}{f(r)} \right]. \quad (2.14)
$$

Therefore, we have

$$
\frac{G_N L}{2V_{d-1}} \mathcal{C} = \int_{r_{\min}}^{r_\infty} dr \left[\frac{\sqrt{P_v^2 + f(r)a^2(r)(\frac{r}{L})^{2(d-1)}}}{f(r)} - \frac{P_v}{f(r)} \right]
$$
$$
+ P_v \left[\frac{\tau}{2} + r_*(r_\infty) - r_*(r_{\min}) \right]. \quad (2.15)
$$

Next, we can take the time derivative of Eq. (2.15):

$$
\frac{G_N L}{2V_{d-1}} \frac{d\mathcal{C}}{d\tau}
$$
$$
= \frac{dP_v}{d\tau} \int_{r_{\min}}^{r_\infty} dr \left[\frac{P_v}{f(r)\sqrt{P_v^2 + f(r)a^2(r)(\frac{r}{L})^{2(d-1)}}} - \frac{1}{f(r)} \right]
$$
$$
+ \frac{dP_v}{d\tau} \left[\frac{\tau}{2} + r_*(r_\infty) - r_*(r_{\min}) \right] + \frac{P_v}{2}. \quad (2.16)
$$

We notice that the same term as in Eq. (2.13) appears in Eq. (2.16), which can greatly simplify the equation, that is,

$$
\frac{d\mathcal{C}}{d\tau} = \frac{V_{d-1}}{G_N L} P_v. \quad (2.17)
$$

Therefore, the growth rate of the complexity is proportional to the conserved momentum P_v. Because of $r_* = -\int_r^\infty \frac{dr'}{f(r')}$, we can get the expression of the boundary time by Eq. (2.13):

$$
\tau = -2 \int_{r_{\min}}^\infty dr \frac{P_v}{f(r)\sqrt{P_v^2 + f(r)a^2(r)(\frac{r}{L})^{2(d-1)}}}
$$
$$
= -2 \int_{r_{\min}}^\infty dr \frac{P_v}{f(r)\sqrt{P_v^2 - U(r)}}. \quad (2.18)
$$

When $\tau \to \infty$, we let the $U(r_f) = P_\infty$, so we have

$$
\frac{d\mathcal{C}}{d\tau}\bigg|_{\tau\to\infty} = \frac{V_{d-1}}{G_N L} P_\infty. \quad (2.19)
$$

III. HOLOGRAPHIC COMPLEXITY FOR BLACK HOLES WITH A SINGLE HORIZON

In this section, we will take the planar AdS black hole and the five-dimensional Gauss-Bonnet-AdS black hole as examples to discuss the generalized volume complexity for the black holes with a single horizon and a spacelike curvature singularity. We find that in such a case the turning time still exists and may not be unique. On the other hand, for the five-dimensional Gauss-Bonnet-AdS black hole, we find that the shape of the effective potential can determine whether the parameter space of the coupling constant is the full space.

A. Planar AdS black hole

There are some examples of $a(r)$ presented in Ref. [35]. In this section, we expand on the authors' examples and consider the turning time in each other. We also use the Weyl tensor for the bulk spacetime to construct the

gravitational observable on the codimension-1 extremal slice Σ. That is,

$$a(r) = 1 + \sum_{j=1}^{N}(-1)^j\lambda_j(L^4C^2)^j, \tag{3.1}$$

$$C^2 \equiv R_{\mu\nu\sigma\rho}R^{\mu\nu\sigma\rho} - \frac{4}{d-1}R_{\mu\nu}R^{\mu\nu} + \frac{2}{d(d-1)}R$$

$$= d(d-1)^2(d-2)\frac{r_h^{2d}}{L^4r^{2d}}, \tag{3.2}$$

where $C^2 \equiv C_{\mu\nu\sigma\rho}C^{\mu\nu\sigma\rho}$ denotes the square of the Weyl tensor for the bulk spacetime, λ_j are dimensionless coupling constants, and $j = 1, 2, ..., N$. To simplify the calculation, we set $\tilde{\lambda}_j = [d(d-1)^2(d-2)]^j\lambda_j$. After this substitution, $a(r)$ can be rewritten as

$$a(r) = 1 + \sum_{j=1}^{N}(-1)^j\tilde{\lambda}_j\left(\frac{r_h}{r}\right)^{2dj}. \tag{3.3}$$

When all $\lambda_j = 0$, we have $a(r) = 1$, which corresponds to the CV proposal. The case of $N = 1$ was discussed in Ref. [33]. We begin our analysis with $N = 2$, i.e.,

$$a(r) = 1 - \tilde{\lambda}_1\left(\frac{r_h}{r}\right)^{2d} + \tilde{\lambda}_2\left(\frac{r_h}{r}\right)^{4d}. \tag{3.4}$$

It was chosen in Ref. [35] to make the extreme surface approach the singularity. Then, we can obtain the expression of the effective potential, i.e.,

$$U(r) = -r^{-d}\left(\frac{r}{L}\right)^{2d}(r^d - r_h^d)\left[1 - \left(\frac{r_h}{r}\right)^{2d}\tilde{\lambda}_1 + \left(\frac{r_h}{r}\right)^{4d}\tilde{\lambda}_2\right]^2. \tag{3.5}$$
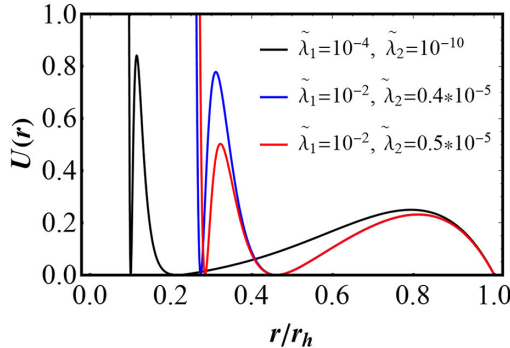
We consider the case of $d = 3$ and choose appropriate value of the coupling parameter $\tilde{\lambda}_j$ as shown in Fig. 2(b). In the red area, $U(r)$ gives two peaks, and their values gradually decrease from left to right. According to Eq. (2.12), we can obtain the expression for the generalized volume, which is given by

$$V_{\text{gen}} = V_{d-1}\int_{r_{\text{min}}}^{r_\infty}\frac{a^2(r)(\frac{r}{L})^{2(d-1)}}{\sqrt{Pv^2 - U(r)}}dr. \tag{3.6}$$

By calculating the generalized volume, we can observe its correspondence with P_v as shown in Fig. 3(b). When we select the appropriate value of λ to construct the $U(r)$ as shown in Fig. 2(a), there are two local maxima of the effective potential. Equation (2.17) tells us that a higher peak corresponds to a larger growth rate of the generalized volume complexity. Therefore, at a very late time, the generalized volume corresponding to the peak on the left must be bigger than that of the right. Interestingly, as shown in Fig. 3(a), the shorter peak corresponds to a larger generalized volume over a significant range. Consequently, there must be a moment when the generalized volumes corresponding to the left and right peaks are equal, and after that, the relative size relationship between these two will reverse. We refer to this moment as the turning time [37].

By selecting different values of $\tilde{\lambda}_1$ and $\tilde{\lambda}_2$, we can get the corresponding relationship between the parameters and the turning time, as shown in Fig. 4. In another paper, we investigated the turning time for the four-dimensional RN-AdS black hole [37].

We discovered that the turning time has a logarithmic dependence on its parameter, and we have determined the fitting function to be given by

$$\tau_{\text{turning}} = a_1 - b_1\ln(\tilde{\lambda}_1 + c_1), \tag{3.7}$$

(a) The effective potential defined in Eq. (3.5).
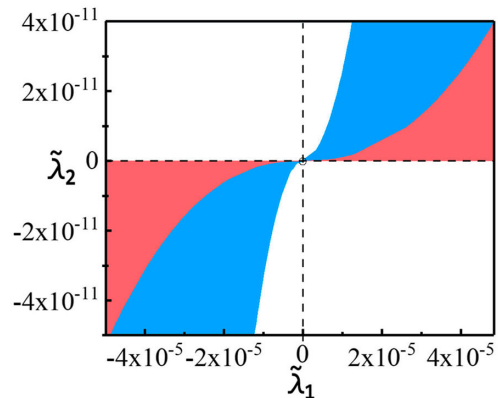
(b) The parameter space of $\tilde{\lambda}_1$ and $\tilde{\lambda}_2$.

FIG. 2.   (a) The image of the effective potential $U(r)$ with different coupling constants. (b) In the red area, the effective potential has two local maxima, and the left one is larger than the right one. In the blue area, there are also two local maxima, but the local maxima on the right is greater than the one on the left.
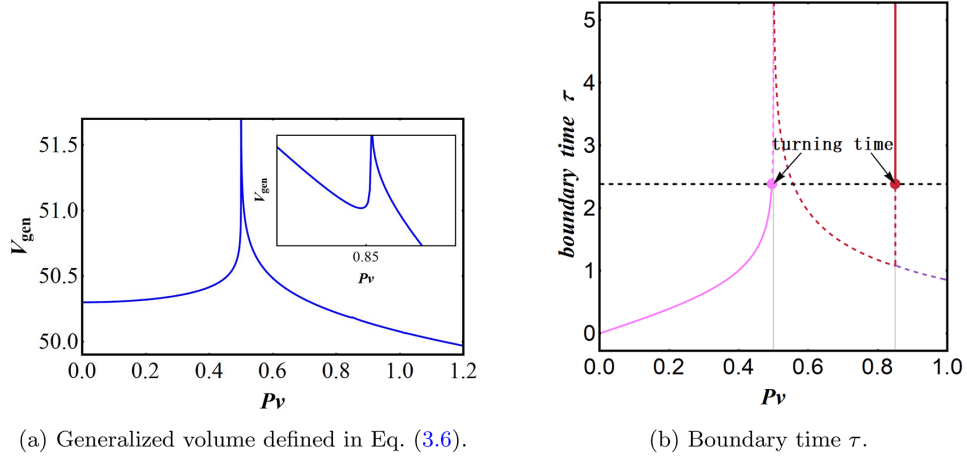
(a) Generalized volume defined in Eq. (3.6).

(b) Boundary time τ.

FIG. 3. (a) The relation between the generalized volume and the conserved momentum P_v of the planar AdS black hole with $d = 3, \frac{r_h}{L} = 1, \tilde{\lambda}_1 = 10^{-4}, \tilde{\lambda}_2 = 1.1 * 10^{-10}$. The part outside the horizon grows linearly with r and diverges at infinity, we just cut it off at $r = 10 r_h$. (b) The relation between the boundary time τ and the conserved momentum P_v using the parameters mentioned in (a). The two solid gray lines represent the two local maxima of $U(r)$, i.e., $U(r_f)$. The pink curve corresponds to the right peak, the red curve corresponds to the left one, and the purple curve corresponds to the divergent branch on the left. Both the pink and red solid lines represent larger generalized volumes at the corresponding boundary time, while the dotted lines are the opposite.
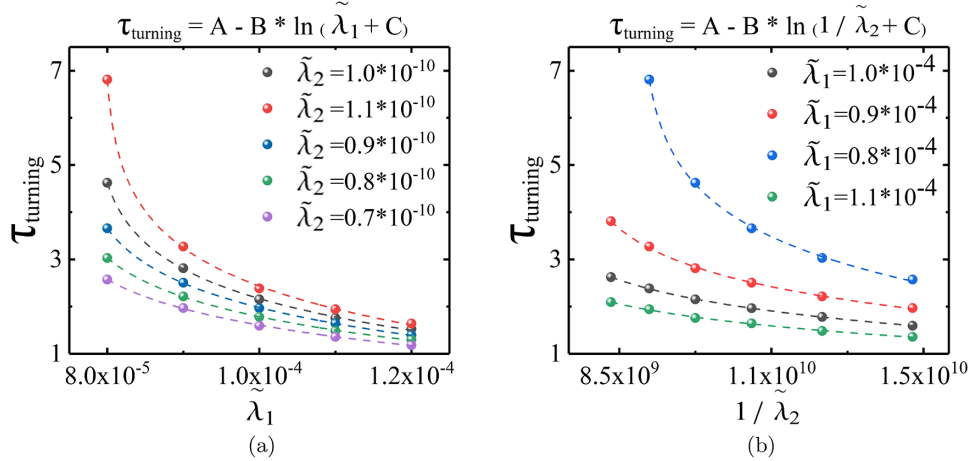

FIG. 4. The fitting of turning time on $\tilde{\lambda}_1$ and $\tilde{\lambda}_2$.

$$\tau_{\text{turning}} = a_2 - b_2 \ln(1/\tilde{\lambda}_2 + c_2), \qquad (3.8)$$

where a_i, b_i, and c_i are the fitting values. Among them, a_i and b_i have dimensions of length, while c_i are dimensionless constants.

Similarly, we can also consider polynomials with three monomials or even more. Choosing $N = 3$, we can get

$$a(r) = 1 - \tilde{\lambda}_1 \left(\frac{r}{L}\right)^{2d} + \tilde{\lambda}_2 \left(\frac{r}{L}\right)^{4d} - \tilde{\lambda}_3 \left(\frac{r}{L}\right)^{6d}, \qquad (3.9)$$

$$U(r) = -r^{-d} \left(\frac{r}{L}\right)^{2d} (r^d - r_h^d) \left[1 - \left(\frac{r_h}{r}\right)^{2d} \tilde{\lambda}_1 \right.$$
$$\left. + \left(\frac{r_h}{r}\right)^{4d} \tilde{\lambda}_2 - \left(\frac{r_h}{r}\right)^{6d} \tilde{\lambda}_3 \right]^2. \qquad (3.10)$$

As before, we continue to consider the planer black hole in $(3 + 1)$-dimensional spacetime. Choosing different values of the parameters, we may have from 0 to 3 local maxima of the effective potential, as shown in the left image of Fig. 5. In this case, there are three growth rates at late time. However, the number of turning times does not necessarily have to be 2, as shown in the right image of Fig. 5. The highest peak is so steep that the middle peak corresponds to a generalized volume that can never be the largest. On the other hand, if we select more extreme parameters such that the heights of the two peaks on the left and middle are very close to each other, we can identify a second turning time, as shown in Fig. 6.

The emergence of the turning time shows that the growth rate of the complexity is abrupt while the complexity itself is still continuous. This phenomenon may imply that there
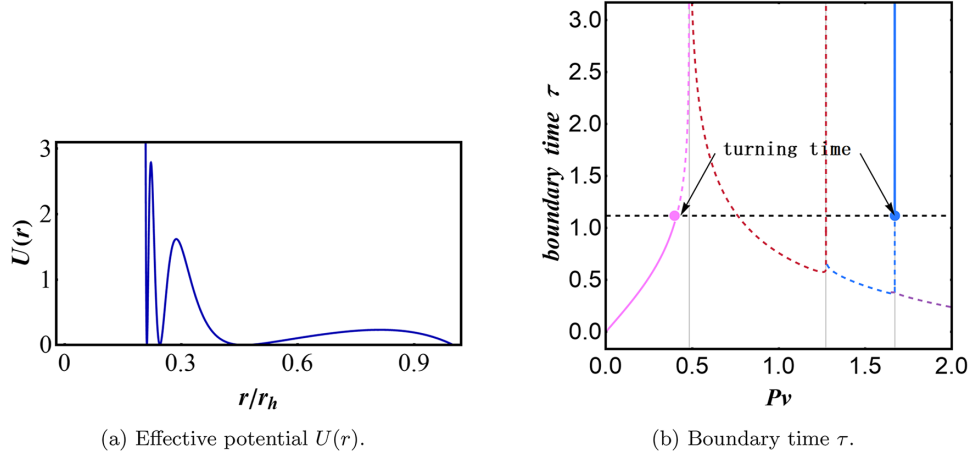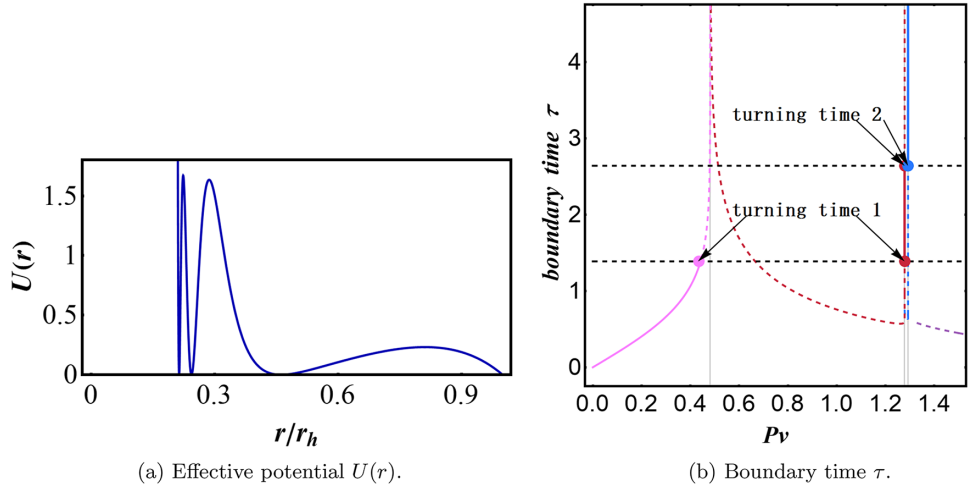
(a) Effective potential $U(r)$.

(b) Boundary time τ.

FIG. 5.   (a) The image of the effective potential $U(r)$ with $L = 1$, $\tilde{\lambda}_1 = 10^{-2}$, $\tilde{\lambda}_2 = 3 * 10^{-6}$, and $\tilde{\lambda}_3 = 1.9 * 10^{-10}$. (b) The relation between the boundary time τ and the conserved momentum P_v using the parameters mentioned in (a). The three solid gray lines represent the three local maxima of $U(r)$, i.e., $U(r_f)$. The pink, red, and blue curves correspond to the right, middle, and left peaks, respectively, and the purple curve corresponds to the divergent branch on the left. Both the pink and blue solid lines represent larger generalized volumes at the corresponding boundary time, while the dotted lines are the opposite.

(a) Effective potential $U(r)$.

(b) Boundary time τ.

FIG. 6.   (a) The image of the effective potential $U(r)$ with $L = 1$, $\tilde{\lambda}_1 = 10^{-2}$, $\tilde{\lambda}_2 = 3 \times 10^{-6}$. and $\tilde{\lambda}_3 = 1.967 \times 10^{-10}$. (b) The relation between the boundary time τ and the conserved momentum P_v using the parameters mentioned in (a). The three solid gray lines represent the three local maxima of $U(r)$, i.e., $U(r_f)$. The pink, red, and blue curves correspond to the right, middle, and left peaks, respectively, and the purple curve corresponds to the divergent branch on the left. The pink, red, and blue solid lines represent larger generalized volumes at the corresponding boundary time, while the dotted lines are the opposite.

are phase transitions and may mean that the shortest geodesic between the reference state and the target state will change. Similar phase transitions have also been observed in quantum computation complexity [54,64–66] and holographic complexity [67–69].

B. Five-dimensional Gauss-Bonnet-AdS black hole

In Ref. [38], the authors analyzed the four-dimensional and five-dimensional Gauss-Bonnet-AdS black hole and found that there is a turning time for the four-dimensional Gauss-Bonnet-AdS black hole, which has two horizons and for which the extremal hypersurfaces are confined between

them. In this subsection, we will delve deeper into this issue and examine the distinctions among various gravitational observables. The metric of the five-dimensional Gauss-Bonnet-AdS black hole is given by Ref. [70],

$$ds^2 = -f(r)dv^2 + 2dvdr + r^2 d\Omega_3^2, \qquad (3.11)$$

where

$$f(r) = 1 + \frac{r^2}{2\alpha}\left[1 - \sqrt{1 + 8\alpha\left(\frac{m}{r^4} - \frac{1}{L^4}\right)}\right], \qquad (3.12)$$

α is a coupling constant with dimensions of length squared, and $m \equiv 16\pi GM/(d-2)\Omega_{d-2}$ represents the re-scaled mass of the black hole. We can easily obtain the effective potential, i.e.,
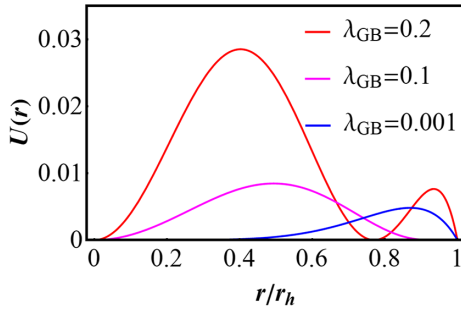
$$U(r) = -f(r)a^2(r)r^6. \tag{3.13}$$

In this section, we use the Gauss-Bonnet invariant and the Weyl tensor, respectively, to construct $a(r)$. For the Gauss-Bonnet case, we choose

$$a_{\mathrm{GB}}(r) = 1 + \lambda_{\mathrm{GB}}\alpha^2\mathcal{R}_{\mathrm{GB}}, \tag{3.14}$$

where λ_{GB} is the dimensionless coupling constant, and $\mathcal{R}_{\mathrm{GB}}$ is given by

$$\mathcal{R}_{\mathrm{GB}} = \frac{12(2(f(r)-1))f(r)' + rf(r)'^2 + r(f(r)-1)f(r)''}{r^3}. \tag{3.15}$$

The effective potential (3.13) calculated with $a(r)_{GB}$ is shown in Fig. 7.

In this case, the effective potential goes to zero at the singularity. Additionally, since it remains consistently zero on the event horizon and the effective potential is always non-negative in the spacelike region inside the black hole, there is at least one extreme hypersurface at late time. By selecting the appropriate coupling constant λ_{GB}, we can find the turning time as shown in the left image of Fig. 8. It is worth noting that in this case the growth rate of the complexity at late time always exist and is not zero. It has a lower limit when the turning time tends to infinity, as shown in the right image of Fig. 8.

For the Weyl tensor case, there are some discussions in Ref. [38], and we can still find the turning time by adding higher-order terms, i.e.,
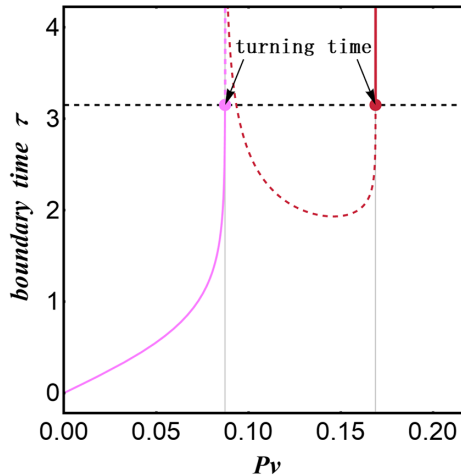
$$a_W(r) = 1 + \lambda_{W_1}L^4C^2 - \lambda_{W_2}L^8C^4, \tag{3.16}$$

where

(a) Effective potential $U(r)$.
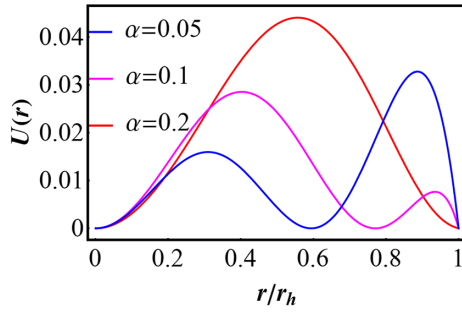
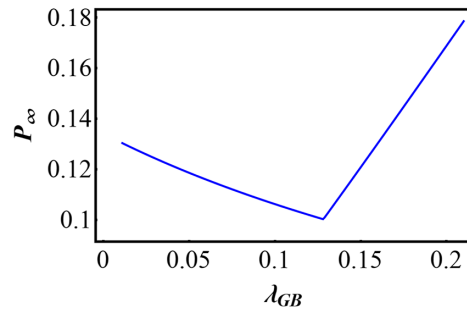
(b) Effective potential $U(r)$.

FIG. 7. The shape of the effective potential. (a) $L = 1$, $m = 1$, $\alpha = 0.1$. (b) $L = 1$, $m = 1$, $\lambda_{\mathrm{GB}} = 0.2$.

(a) Boundary time τ.

(b) Growth rate at late time.

FIG. 8. (a) The relation between the boundary time τ and the conserved momentum P_v with $L = 1$, $m = 1$, $\alpha = 0.1$, $\lambda_{\mathrm{GB}} = 0.2$. (b) The relation between the coupling constant λ and the conserved momentum at late time P_∞ with $L = 1$, $m = 1$, $\alpha = 0.1$.
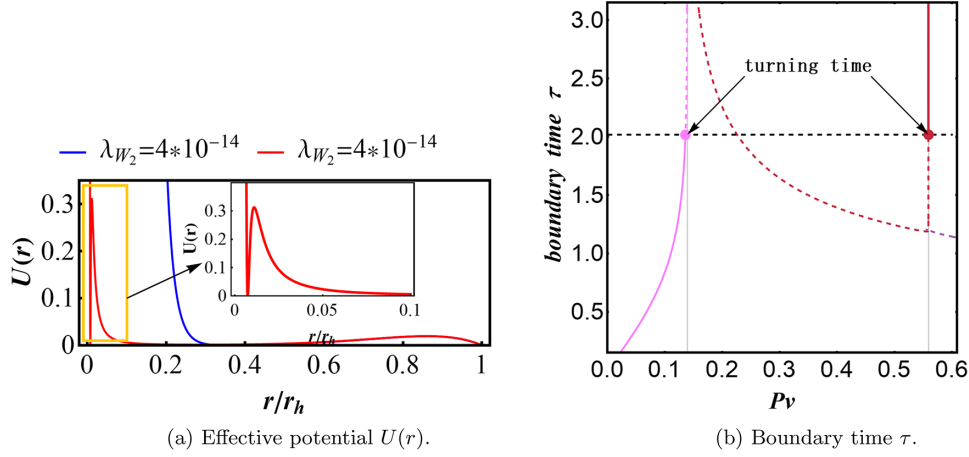
(a) Effective potential $U(r)$.

(b) Boundary time τ.

FIG. 9.   (a) The shape of the effective potential with $L = 1$, $m = 1$, $\alpha = 0.1$, $\lambda_{W_1} = 5 * 10^{-4}$. The red line gives the two peaks that are larger on the left than on the right, the blue line has only one peak, and the black dotted line has no peak. (b) The relation between the boundary time τ and the conserved momentum P_v with $L = 1$, $m = 1$, $\alpha = 0.1$, $\lambda_{W_1} = 5 * 10^{-4}$, $\lambda_{W_1} = 4 * 10^{-14}$.

$$C^2 = \frac{(2 - 2f(r) + 2rf(r)' - r^2 f(r)'')^2}{2r^4}. \qquad (3.17)$$

In this case, the effective potential diverges at a singularity, as shown in the left image of Fig. 9. We can still find the turning time by choosing an appropriate coupling constant λ_W, as shown in the right image of Fig. 9.

For the case where the effective potential is zero at a singularity, the presence of extremal hypersurfaces that cannot reach the late-time regime will no longer occur. As the effective potential is consistently zero at the horizon, if it is also zero at the singularity, there must be at least one local maximum between the horizon and the singularity. This situation is similar to a black hole with two horizons. And when the effective potential diverges at the singularity, the existence of the local maximum depends on the choice of the coupling constant.

In our opinion, the generalized volume complexity can be divided into two categories. In the first category, the effective potential diverges at the singularity, while in the second one, it goes to zero at either the singularity or the Cauchy horizon. For the single horizon black holes without singularity, there exists a third possible scenario for the effective potential, which we consider to be the same as when it diverges at the singularity and thus belong to the first category; see Appendix for details. The first category will make the coupling constant have a limit, which requires that there exists an extremal hypersurface at late time. In the second category, the coupling constants are desirable across the full phase space, as the extreme hypersurfaces capable of evolving at late time always exist. Different values of the coupling constant will only affect the growth rate of the complexity at late time, as well as the presence or absence of the turning time. In this case, the growth rate of the generalized volume complexity will have a lower limit value, but not zero.

IV. HOLOGRAPHIC COMPLEXITY FOR BLACK HOLES WITH TWO HORIZONS

In this section, we take the charged BTZ black hole as an example to calculate its generalized volume complexity for black holes with a Cauchy horizon. In this case, there is no generalized volume complexity of the first category. We will, respectively, use spacetime curvature and matter to construct the gravitational observables. Let us first give the charged BTZ black hole, whose metric is given by Refs. [71,72],

$$ds^2 = -f(r)dt^2 + \frac{dr^2}{f(r)} + r^2 d\theta^2,$$

$$f(r) = -M + \frac{r^2}{L^2} - \pi Q^2 \ln \frac{r}{L}. \qquad (4.1)$$

The metric is asymptotically AdS_3 with radius L. By convention, we set $8G_N \equiv 1$, where G_N is the Newton's constant. The mass and the charge of the black hole are denoted by M and Q, respectively, and can be expressed in terms of the event horizon and the Cauchy horizon $r_\pm$:

$$M = \frac{r_+^2 \ln \frac{r_-}{L} - r_-^2 \ln \frac{r_+}{L}}{L^2 \ln \frac{r_-}{r_+}}, \qquad (4.2)$$

$$Q^2 = \frac{r_+^2 - r_-^2}{\pi L^2 \ln \frac{r_+}{r_-}}. \qquad (4.3)$$

We can also rewrite the metric into the ingoing Eddington-Finkelstein coordinates, that is,

$$ds^2 = -f(r)dv^2 + 2dvdr + r^2 d\theta^2. \qquad (4.4)$$

The generalized volume complexity can be represented by

$$C = 2\pi \int d\sigma r \sqrt{2\dot{v}\,\dot{r} - f(r)\dot{v}^2}\, a(r)$$

$$\equiv \frac{2\pi}{G_N L} \int_\Sigma d\sigma \mathcal{L}(r, \dot{v}, \dot{r}). \qquad (4.5)$$

Obviously, the gauge given by Eq. (2.5) becomes

$$\sqrt{-f(r)\dot{v}^2 + 2\dot{v}\,\dot{r}} = a(r)r. \qquad (4.6)$$

We can just write down its effective potential, complexity, and complexity growth rate:

$$U(r) = -f(r)a^2(r)r^2, \qquad (4.7)$$

$$C = -\frac{4\pi}{G_N L} \int_{r_{\min}}^{\infty} \frac{U(r)}{f(r)\sqrt{U(r_{\min}) - U(r)}} dr, \qquad (4.8)$$

$$\frac{dC}{d\tau} = \frac{2\pi}{G_N L} P_v. \qquad (4.9)$$

A. Generalized volume complexity constructed by spacetime curvature

It is well known that the Weyl tensor is always zero when $d = 2$, so we need to look for other nontrivial scalar functions. In this regard, we can naturally think of the three-dimensional replacement of the Weyl tensor, i.e., the Cotton tensor C_3. In this subsection, we choose $a(r) = 1 + \lambda L^6 C_3^2$, where

$$C_3 = C_{ijk} \equiv \nabla_i R_{jk} - \nabla_j R_{ik} - \frac{1}{4}(\nabla_i R g_{jk} - \nabla_j R g_{ik}) \qquad (4.10)$$

is the Cotton tensor. In the three-dimensional case, $C_3^2 = \frac{1}{4}f(r)f'''(r)^2$. Thus, we can obtain the expression of the effective potential,
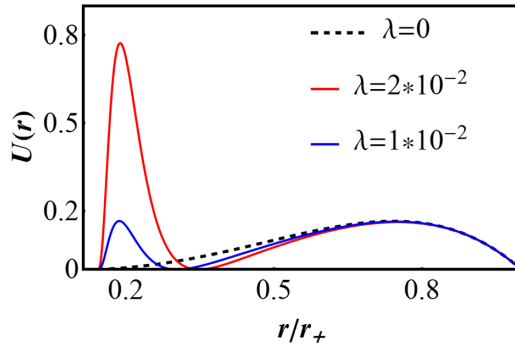
$$U(r) = \left(M - \frac{r^2}{L^2} + \pi Q^2 \ln\frac{r}{L}\right)$$
$$\times \left(r + \lambda \frac{L^6 \pi^2 Q^4 (-M + r^2/L^2 - \pi Q^2 \ln\frac{r}{L})}{r^5}\right)^2. \qquad (4.11)$$

Similarly, we can still get a figure of the effective potential and the corresponding turning time as shown in Fig. 10.

When $q = 0$, the cotton tensor is zero, and generalized volume complexity regresses to the CV proposal.

B. Generalized volume complexity constructed by matter content

For charged black holes, another naturally occurring scalar function can effectively construct the generalized volume complexity. i.e., the electromagnetic field action. In this situation, we choose $a(r) = 1 - \lambda L^2 F_{\mu\nu} F^{\mu\nu}$, where $F_{\mu\nu} F^{\mu\nu} = -2\frac{Q^2}{r^2}$, and can obtain an expression for the effective potential, that is,

$$U(r) = \left(r - \frac{2L^2 Q^2 \lambda}{r}\right)^2 \left(M - \frac{r^2}{L^2} + \pi Q^2 \ln\frac{r}{L}\right). \qquad (4.12)$$

Of course, we can use this configuration to analyze all other charged black holes.

In this case, we can still find a series of λ, Q, and M such that $U(r)$ has more than one local maxima between r_- and r_+; the one with smaller r is also larger. The parameter space is shown in Fig. 11. In the analysis that follows, we only consider the parameters that fall within the red areas, where we have two local maxima that decrease sequentially from left to right. As before, we consider their turning time. For the example shown in Fig. 12, the boundary time and turning time can be reflected in Fig. 13.

(a) Effective potential $U(r)$.
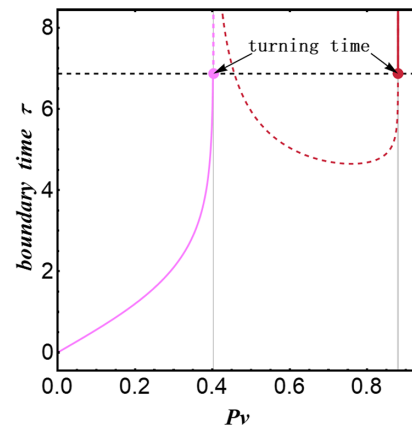
(b) Boundary time τ.

FIG. 10. Left: the shape of the effective potential with $L = M = 1$ and $Q = 0.4$. Right: the relation between the boundary time τ and the conserved momentum P_v with $\lambda = 2 * 10^{-2}$, $L = M = 1$, and $Q = 0.4$.
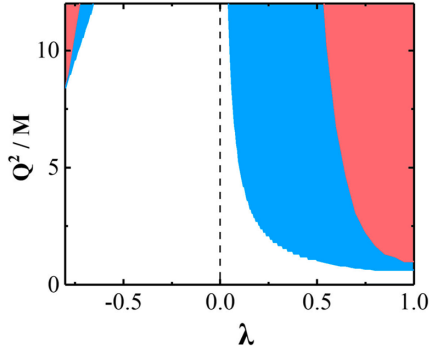
FIG. 11. The parameter space of the effective potential $U(r)$ between the two horizons of the charged BTZ black hole. In the red area, there are two local maxima that decrease from left to right. In the blue area, there are also two local maxima, but the local maximum on the right is greater than the one on the left. In the remaining white area, there is only one local maximum.

We fix $M = L = 1$ and choose different $\frac{Q^2}{M}$ or λ to construct a series of $U(r)$ as shown in Fig. 14, in which we only consider the case that the effective potential has two local maxima. It is worth mentioning that when we fix $M = L$, r_- varies monotonically with $\frac{Q^2}{M}$ as shown in the right figure of Fig. 14. The turning time of the complexity is still logarithmic with its parameter,

$$\tau_{\text{turning}} = A_{QM} - B_{QM} \ln\left(\frac{M}{Q^2} + C_{QM}\right),$$

$$\tau_{\text{turning}} = A_\lambda - B_\lambda \ln(\lambda + C_\lambda), \tag{4.13}$$

where A, B, and C are the fitting values. Among them, A and B have length dimensions, and C is a dimensionless constant. This conclusion is similar to that of constructing

(a) Boundary tims τ.
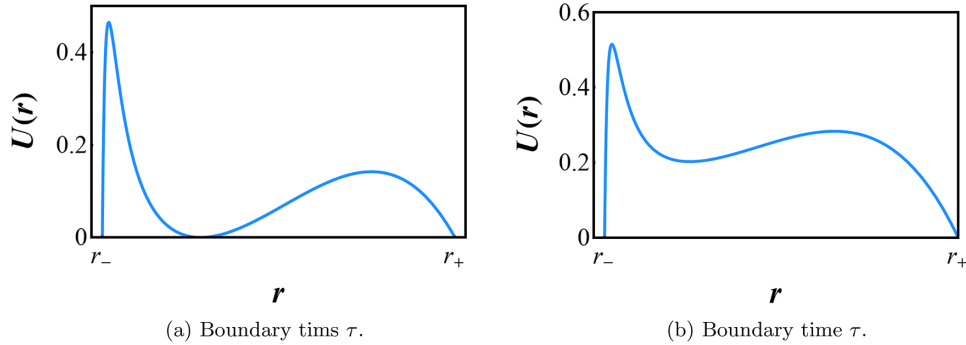

(b) Boundary time τ.

FIG. 12. The effective potential defined in Eq. (4.12). In this situation, we may have 1 or 2 local maxima of the effective potential for different parameters. When the number of the local maxima is 1, the result is similar to the CV proposal. Therefore, we only consider the case of two local maxima. Left: the shape of the effective potential for $\lambda = 0.5$, $L = M = 1$, and $Q = 0.3$. There are two local maxima and the local minimum between them is zero. Right: the shape of the effective potential for $\lambda = -0.5$, $L = M = 1$, and $Q = 0.3$. There are also two local maxima, but the minimum between them does not reach zero. Whether the local minimum is zero depends only on the positive or negative of λ.
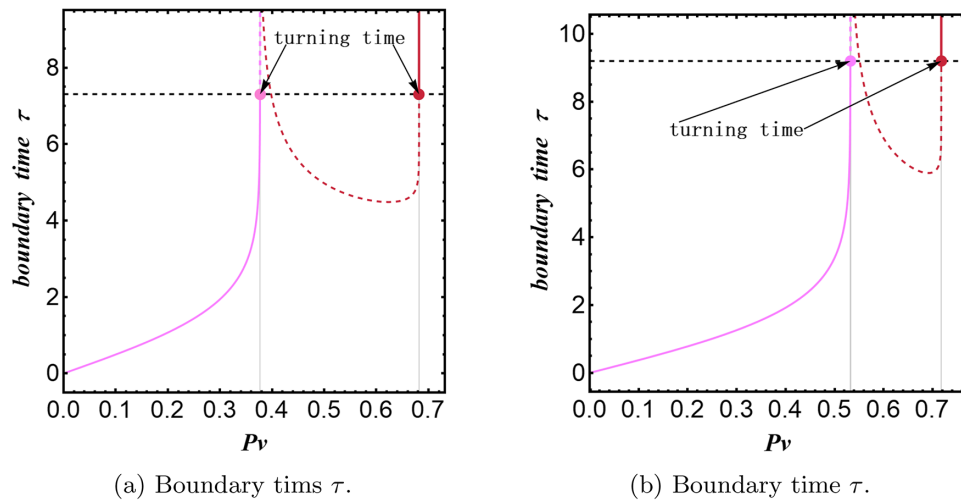

(a) Boundary tims τ.

(b) Boundary time τ.

FIG. 13. The relation between the boundary time τ and the conserved momentum P_v. (a) $\lambda = 0.5$, $L = M = 1$, and $Q = 0.3$. (b) $\lambda = -0.5$, $L = M = 1$, and $Q = 0.3$.

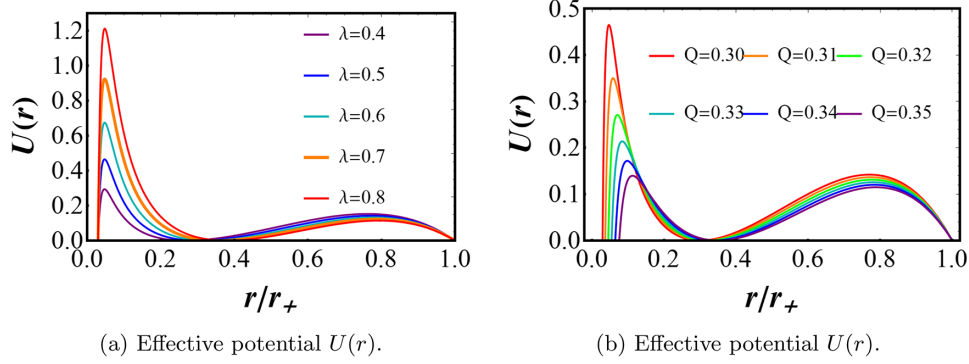(a) Effective potential $U(r)$.

(b) Effective potential $U(r)$.

FIG. 14. The shape of the effective potential with $L = M = 1$. (a) $\lambda = 0.4$ to 0.8 and $Q = 0.3$. (b) $Q = 0.30$ to 0.35 and $\lambda = 0.5$.

C. RN-AdS black hole rediscussion

In our previous work [37], we considered the four-dimensional RN-AdS black hole as an example to find the turning time. However, it is important to note that the conclusion regarding the RN-AdS black hole does not necessarily converge to that of the AdS-Schwarzschild black hole. Therefore, we continue our research using the metric under the Eddington-Finkelstein coordinate, denoted as

$$ds^2 = -f(r)dv^2 + 2dvdr + r^2 d\Omega^2, \tag{4.14}$$

$$
\begin{aligned}
f(r) &= 1 - \frac{2M}{r} + \frac{Q^2}{r^2} + \frac{r^2}{L^2} \\
&= \frac{(r-r_1)(r-r_2)(L^2+r^2+r_1^2+r_2^2+r_1 r_2+r(r_1+r_2))}{r^2 L^2},
\end{aligned} \tag{4.15}
$$

where

$$M = \frac{(r_1+r_2)(L^2+r_1^2+r_2^2)}{2L^2}, \tag{4.16}$$

$$Q = \frac{\sqrt{r_1 r_2 (L^2 + r_1^2 + r_1 r_2 + r_2^2)}}{L}. \tag{4.17}$$

The solution to the equation of motion remains unchanged from before, and we can get the expression of the effective potential $U(r) = -f(r)a^2(r)r^4$. We still use the Weyl tensor to construct the gravitational observable, i.e.,

$$a(r) = 1 + \lambda L^4 C^2, \tag{4.18}$$

$$C^2 = \frac{(2 - 2f(r) + 2rf'(r) - r^2 f''(r))^2}{3r^4}. \tag{4.19}$$

Now, we can fix the event horizon and adjust Q so that the Cauchy horizon gradually approaches the singularity, meanwhile the peak on the left also approaches the singularity, as shown in the left image of Fig. 15. When $Q \to 0$, the Cauchy horizon will be infinitely close to the singularity. At the same time, the left peak still has a finite maximum value that depends on the coupling constant λ. However, if $Q = 0$, the black hole returns to the Schwarzschild-AdS black hole. With the disappearance of the Cauchy horizon, the left peak disappears together, and the effective potential diverges at the singularity. In other words, in the configuration we are considering, as the charge Q disappears, the second category of the generalized volume complexity transitions to the first generalized volume complexity with spacetime curvature discussed in Sec. III.
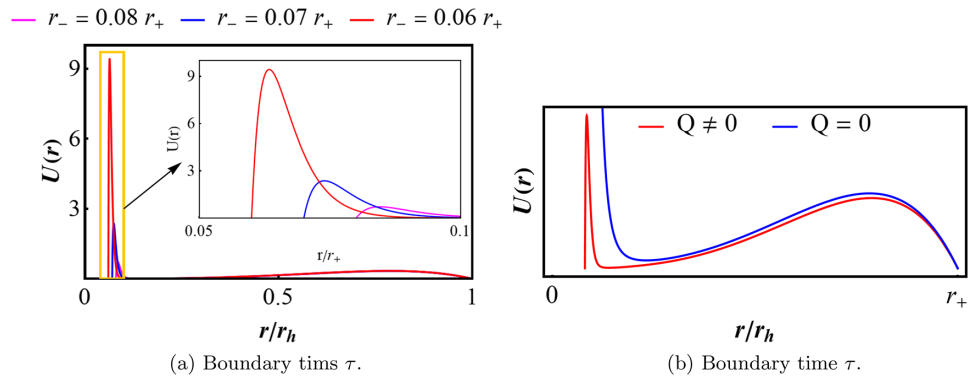

(a) Boundary tims τ.

(b) Boundary time τ.

FIG. 15. (a) The shape of the effective potential with $L = r_+ = 1$, $\lambda = 1 * 10^{-6}$. (b) The comparison of $Q \to 0$ and $Q = 0$.

case. This mutation in the growth rate of complexity at late time is shown in the right image of Fig. 15. This brings us back to the Schwarzschild situation, where the coupling constant no longer holds in the full parameter space.

V. $F_1 \neq F_2$

In this section, we will consider the case where $F_1 \neq F_2$. We determine the extreme hypersurface by setting $F_2 = a_2(r)$ and consider the gravitational observables constructed using $F_1 = a_1(r)$, as shown in Eqs. (1.4) and (1.5). Taking the $(d+1)$-dimensional AdS spherically symmetric black hole as an example, we can still use the method in Sec. II to get the conserved momentum and effective potential, i.e.,

$$\dot{r}^2 + U_2(r) = P_v^2, \qquad U_2(r) = -f(r)a_2^2(r)r^{2(d-1)}. \quad (5.1)$$

The anchored boundary time τ is uniquely determined by the properties of the hypersurface, so τ is only related to $a_2(r)$, i.e.,
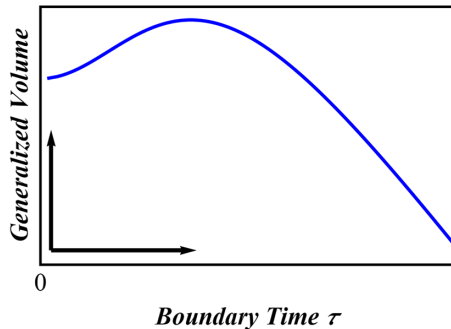
$$\tau = -2 \int_{r_{\min}}^{\infty} dr \, \frac{P_v}{f(r)\sqrt{P_v^2 - U_2(r)}}$$

$$= -2 \int_{r_{\min}}^{\infty} dr \, \frac{\sqrt{U_2(r_{\min})}}{f(r)\sqrt{U_2(r_{\min}) - U_2(r)}}. \quad (5.2)$$

However, the generalized volume complexity will depend on both $a_1(r)$ and $a_2(r)$, that is,

$$\mathcal{C}_{F_1, \Sigma_{F_2}} = \frac{2V_{d-1}}{G_N L} \int_{r_{\min}}^{\infty} \frac{a_1(r)a_2(r)r^{2(d-1)}}{\sqrt{P_v^2 + f(r)a_2^2(r)r^{2(d-1)}}} dr. \quad (5.3)$$

A. Restriction of $a(r)$

We still take the five-dimensional Gauss-Bonnet-AdS black hole as an example and select Eqs. (3.14) and (3.16) as $a_1(r)$ and $a_2(r)$, respectively. Using Eqs. (5.2) and (5.3),

we find that the generalized volume complexity loses the property of late linear growth, as shown in Fig. 16; we think this is unreasonable. The reason for this is that when $a(r)^2$ is replaced by $a_1(r)a_2(r)$ the integrand of $\mathcal{C}$ is no longer positive inside the event horizon. So, we need to impose certain restrictions on $a(r)$. The modified $a(r)$ will ensure that the integrand of $\mathcal{C}$ is always positive inside the event horizon, i.e.,

$$a_1(r) \equiv \sqrt{a_{GB}^2(r)} = |1 + \lambda_{GB}\alpha^2 \mathcal{R}_{GB}|,$$

$$a_2(r) \equiv \sqrt{a_W^2(r)} = |1 + \lambda_{W_1}L^4 C^2 - \lambda_{W_2}L^8 C^4|. \quad (5.4)$$

where the parameters and scalar functionals we choose are consistent with those in Sec.. III B. In this premise, if we order $U_1(r) = -f(r)a_1^2(r)r^{2(d-1)}$, Eq. (5.3) can be rewritten as

$$\mathcal{C}_{F_1, \Sigma_{F_2}} = -\frac{2V_{d-1}}{G_N L} \int_{r_{\min}}^{\infty} \frac{\sqrt{U_1(r)U_2(r)}}{f(r)\sqrt{P_v^2 - U_2(r)}} dr. \quad (5.5)$$

This conclusion is consistent with what Ref. [33] discusses. And its growth rate is only analytically solved at a later stage, i.e.,

$$\lim_{\tau \to \infty} \frac{d\mathcal{C}_{F_1, \Sigma_{F_2}}}{d\tau} = \frac{V_{d-1}}{G_N L} \sqrt{U_1(r_f)}. \quad (5.6)$$

It is worth noting that when $r_{\min} \to r_f$, $U_2(r)$ is at the local maximum, but the value of the growth rate is determined by $U_1(r)$ as shown in Fig. 17. We can still find the turning time in this situation, as shown in the right figure of Fig. 18. Naturally, we can also exchange $a_1(r)$ and $a_2(r)$, i.e.,

$$a_1(r) \equiv \sqrt{a_W^2(r)} = |1 + \lambda_{W_1}L^4 C^2 - \lambda_{W_2}L^8 C^4|, \quad (5.7)$$

$$a_2(r) \equiv \sqrt{a_{GB}^2(r)} = |1 + \lambda_{GB}\alpha^2 \mathcal{R}_{GB}|, \quad (5.8)$$

and can still obtain the turning time as shown in Fig. 19.

(a) The surface far from the singularity.
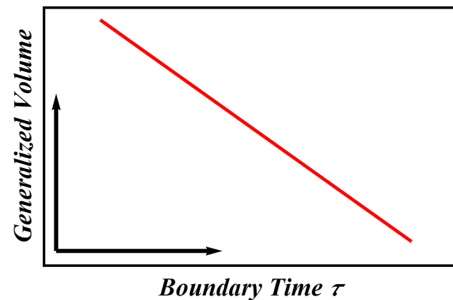
(b) The surface close to the singularity.

FIG. 16.   The relation between the boundary time τ and the generalized volume complexity $\mathcal{C}$ for the case of $F_1 \neq F_2$ with $L = 1$, $m = 1, \alpha = 0.1, \lambda_{GB} = 0.3, \lambda_{W_1} = 0.5 \times 10^{-2}$, and $\lambda_{W_2} = 0.5 \times 10^{-7}$. The blue and red curves correspond to two extreme hypersurfaces that can evolve to the late time. When $\tau \to \infty$, $r_{\min}$ is r_{f_R} and r_{f_L}, respectively.

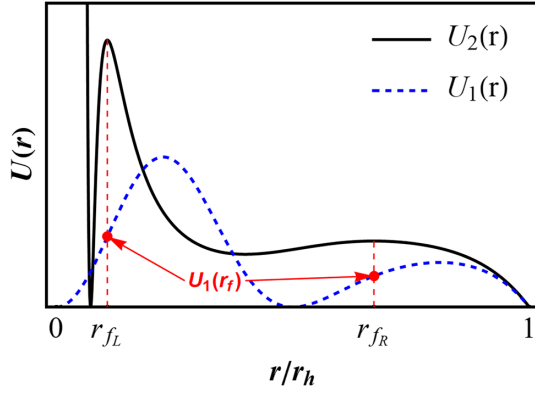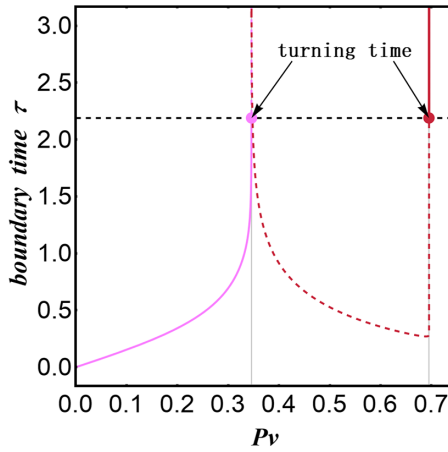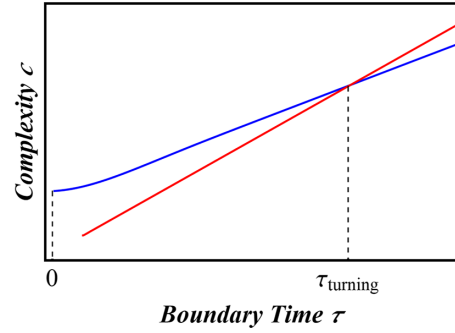FIG. 17. The shape of the effective potential for the case of $F_1 \neq F_2$ with $L = 1$, $m = 1$, $\alpha = 0.01$, $\lambda_{\mathrm{GB}} = 0.3$, $\lambda_{W_1} = 0.3 \times 10^{-3}$, and $\lambda_{W_2} = 0.3 \times 10^{-10}$.

B. Differences from $F_1 = F_2$

For the case of $F_1 \neq F_2$, since the generalized volume depends on the two different scalar functions, $a_1(r)$ and $a_2(r)$, a higher peak no longer necessarily corresponds to an extremal hypersurface with a larger generalized volume as shown in Fig. 20, in which we follow the scalar function defined by Eqs. (5.7) and (5.8). For this case, the generalized volume corresponding to the left peak will never exceed that of the right, even if it is higher. On the other hand, unlike $F_1 = F_2$, the evolution of the generalized volume complexity over time may not be monotonous as shown in Fig. 21; this does not affect the linear growth at late time.
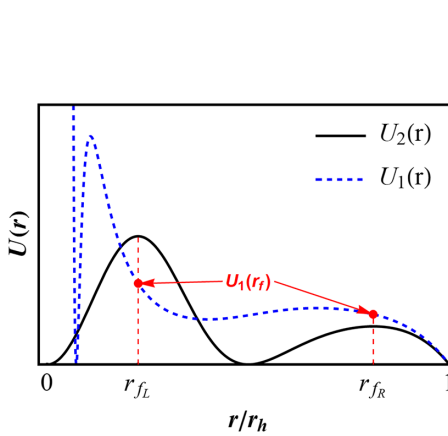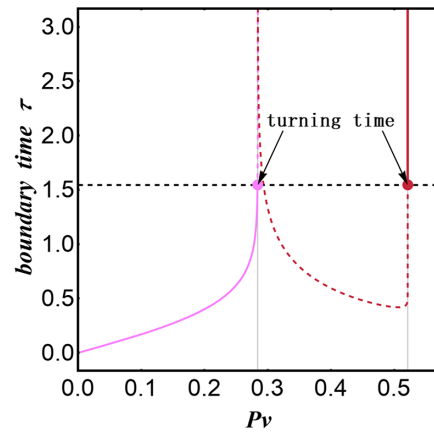

(a) Boundary time τ.

(b) Generalized volume growth

FIG. 18. The figure of the growth of generalized volume complexity with time and the turning time for the case of $F_1 \neq F_2$ with $L = 1$, $m = 1$, $\alpha = 0.01$, $\lambda_{\mathrm{GB}} = 0.3$, $\lambda_{W_1} = 0.3 \times 10^{-3}$, and $\lambda_{W_2} = 0.3 \times 10^{-10}$. (a) The relation between the boundary time τ and the conserved momentum P_v. (b) Generalized volume-complexity evolution over time.

(a) Effective potential $U(r)$.

(b) Boundary time τ.

FIG. 19. The evolution of the generalized volume complexity over time after swapping $a_1(r)$ and $a_2(r)$ in Fig. 17. (a) The effective potential for the case of $F_1 \neq F_2$ with $L = 1$, $m = 1$, $\alpha = 0.01$, $\lambda_{\mathrm{GB}} = 0.3$, $\lambda_{W_1} = 0.3 \times 10^{-3}$, and $\lambda_{W_2} = 0.3 \times 10^{-10}$. (b) The relation between the boundary time τ and the conserved momentum P_v.

(a) Effective potential $U(r)$.

(b) Generalized volume growth

FIG. 20.   (a) The effective potential for the case of $F_1 \neq F_2$ with $L = 1$, $m = 1$, $\alpha = 0.01$, $\lambda_{\mathrm{GB}} = 1$, $\lambda_{W_1} = 10^{-4}$, and $\lambda_{W_2} = 10^{-12}$. (b) Generalized volume-complexity evolution over time with the above parameters.

(a) Effective potential $U(r)$.

(b) Generalized volume growth.
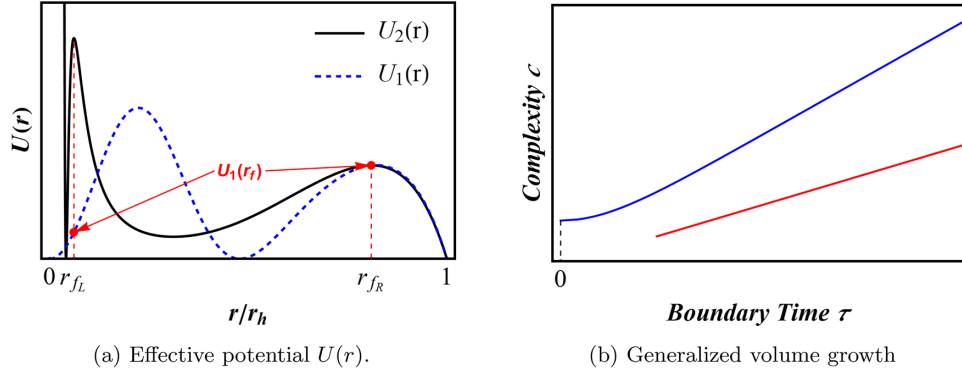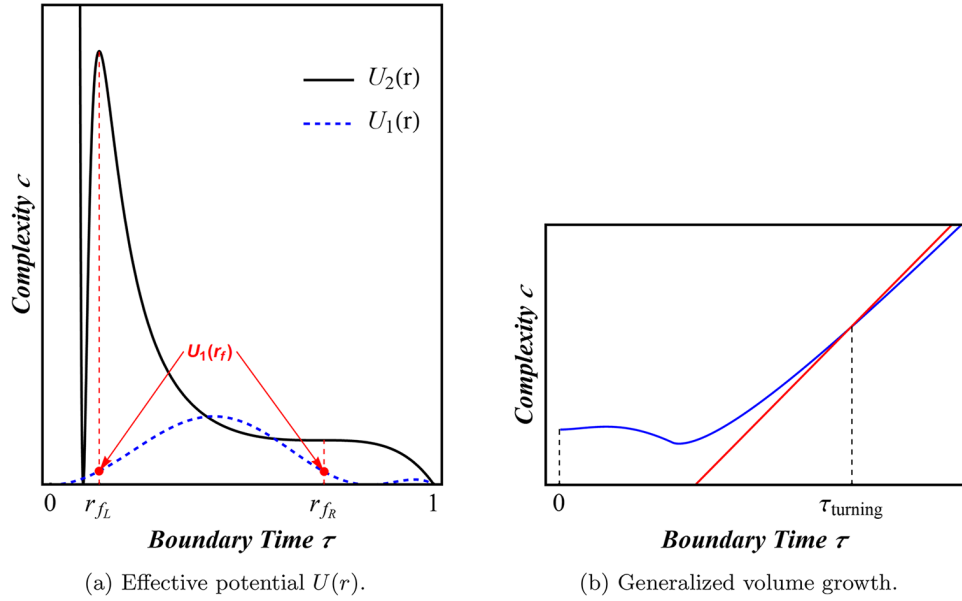
FIG. 21.   (a) The effective potential for the case of $F_1 \neq F_2$ with $L = 1$, $m = 1$, $\alpha = 0.1$, $\lambda_{\mathrm{GB}} = 0.3$, $\lambda_{W_1} = 0.7 \times 10^{-2}$, and $\lambda_{W_2} = 10^{-8}$. (b) Generalized volume-complexity evolution over time with the above parameters.

VI. CONCLUSIONS

In this paper, we considered the generalized volume complexity for the planar AdS black hole, the five-dimensional Gauss-Bonnet-AdS black hole, the charged BTZ black hole, and again discussed the four-dimensional RN-AdS black hole. We derived the expressions for the complexity, Eq. (2.12), and the growth rate of complexity, Eq. (2.17). The growth rate of complexity is directly proportional to the conserved momentum P_v. We used some different scalar functions $a(r)$ to construct various gravitational observables. Through this process, we discovered that the effective potentials exhibit diverse behaviors depending on the choice of $a(r)$, which corresponds to different behaviors in the growth rate of complexity.

In the case we analyzed, there are two or more local maxima for the effective potential. Through numerical integration to solve inversely the boundary times with Eq. (2.18), we observed that in the $P_v - \tau$ diagram multiple P_v values can intersect at the same boundary time τ. It means there are multiple extremal hypersurfaces that anchor to the same boundary time. We chose the one with the largest generalized volume as the dual of the complexity. However, the relative sizes of the generalized volumes are not fixed; the smaller one would "surpass" at a certain moment. We refer to this moment as the turning time. It is worth mentioning that the existence of the turning time does not depend on the spacetime background inside the black hole but can always exist by choosing different gravitational observables. Additionally, the turning time

can occur more than once. Furthermore, we found that the turning time has a logarithmic relationship with the parameters.

In addition, we divided the generalized volume complexity into two categories based on their properties at the singularity or the Cauchy horizon. Different categories determine whether the parameter space is contained within the full parameter space. Further, by taking the four-dimensional RN-AdS black hole as an example, we find that for black holes with two horizons the growth rate of the generalized volume complexity at late time may change discontinuously as the Cauchy horizon disappears.

On the other hand, we find that for the case of $F_1 \neq F_2$, in order to satisfy the property of late-time linear growth of complexity, some restrictions need to be imposed for the scalar function $a(r)$ to ensure that the integrand of the generalized volume complexity remains positive. On this basis, the turning time can still exist; the difference lies in the fact that during the relatively early stages the evolution of complexity with time may not necessarily be monotonic.

Finally, it should be pointed out that we can also consider the complexity equals anything conjecture under the quantum correction, just like the quantum BTZ black hole.

ACKNOWLEDGMENTS

APPENDIX: JT BLACK HOLES

In this Appendix, we will consider briefly about the Jackiw-Teitelboim (JT) black holes, whose matrix is

$$ds^2 = -f(r)dt^2 + \frac{1}{f(r)}dr^2,$$
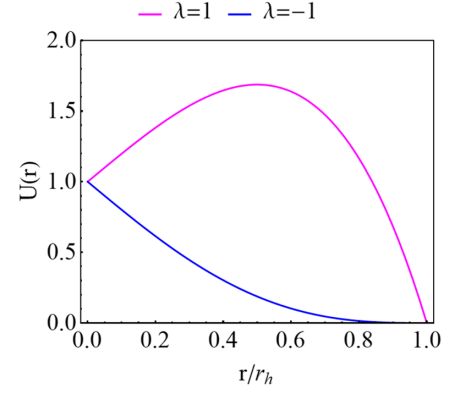$$f(r) = \frac{r^2}{L^2}\left(1 - \frac{r_h^2}{r^2}\right). \tag{A1}$$

FIG. 22. The shape of the effective potential for $L = \phi_h = \phi_0 = 1$. The purple line has one peak, and the blue line has no peak.

It is natural that we can use the dilaton field to construct scalar functions, that is,

$$a(r) = 1 + \lambda \frac{\phi(r)}{\phi_0}, \tag{A2}$$

where

$$\phi(r) = \phi_h \frac{r}{r_h}, \tag{A3}$$

ϕ_0 is a proportionality factor in place of the Newton's constant, and the integration constant ϕ_H is the value of ϕ on the horizon. In this case,

$$U(r) = -f(r)a^2(r), \tag{A4}$$

we can get a shape of the effective potential from this, as shown in Fig. 22. The JT black hole does not have a singularity, and the $f(r)|_{r=0} = r_h^2/L^2$ is a nonzero constant; it results in the effective potential's starting point not being zero or infinity. The characteristics of the effective potential at $r = 0$ depends only on the choice of the scalar functions. However, we think it can be contained by the first category. Whether the effective potential diverges at zero does not by itself affect the extent of the phase space or the size of the local maximum.

[1] J. M. Maldacena, The large N limit of superconformal field theories and supergravity, Adv. Theor. Math. Phys. **2**, 231 (1998).

[2] J. M. Maldacena, TASI 2003 lectures on AdS/CFT, arXiv: hep-th/0309246.

[3] J. Maldacena and L. Susskind, Cool horizons for entangled black holes, Fortschr. Phys. **61**, 781 (2013).

[4] L. Susskind, Copenhagen vs everett, teleportation, and ER = EPR, Fortschr. Phys. **64**, 551 (2016).

[5] L. Susskind, Computational complexity and black hole horizons, Fortschr. Phys. **64**, 24 (2016).

[6] D. Stanford and L. Susskind, Complexity and shock wave geometries, Phys. Rev. D **90**, 126007 (2014).

[7] L. Susskind, Entanglement is not enough, Fortschr. Phys. **64**, 49 (2016).

[8] S. H. Shenker and D. Stanford, Black holes and the butterfly effect, J. High Energy Phys. 03 (2014) 067.

[9] D. A. Roberts, D. Stanford, and L. Susskind, Localized shocks, J. High Energy Phys. 03 (2015) 051.

[10] A. R. Brown, D. A. Roberts, L. Susskind, B. Swingle, and Y. Zhao, Holographic complexity equals bulk action?, Phys. Rev. Lett. **116**, 191301 (2016).

[11] A. R. Brown, D. A. Roberts, L. Susskind, B. Swingle, and Y. Zhao, Complexity, action, and black holes, Phys. Rev. D **93**, 086006 (2016).

[12] J. Couch, W. Fischler, and P. H. Nguyen, Noether charge, black hole volume, and complexity, J. High Energy Phys. 03 (2017) 119.

[13] L. C. Qu, H. Y. Jiang, and Y. X. Liu, Chaos and multifold complexity for an inverted harmonic oscillator, J. High Energy Phys. 12 (2022) 065.

[14] L. C. Qu, J. Chen, and Y. X. Liu, Chaos and complexity for inverted harmonic oscillators, Phys. Rev. D **105**, 126015 (2022).

[15] D. Carmi, R. C. Myers, and P. Rath, Comments on holographic complexity, J. High Energy Phys. 03 (2017) 118.

[16] D. Carmi, S. Chapman, H. Marrochio, R. C. Myers, and S. Sugishita, On the time dependence of holographic complexity, J. High Energy Phys. 11 (2017) 188.

[17] S. Chapman, H. Marrochio, and R. C. Myers, Holographic complexity in Vaidya spacetimes. Part I, J. High Energy Phys. 06 (2018) 046.

[18] S. Chapman, H. Marrochio, and R. C. Myers, Holographic complexity in Vaidya spacetimes. Part II, J. High Energy Phys. 06 (2018) 114.

[19] B. Swingle and Y. Wang, Holographic complexity of Einstein-Maxwell-Dilaton gravity, J. High Energy Phys. 09 (2018) 106.

[20] Z. Fu, A. Maloney, D. Marolf, H. Maxfield, and Z. Wang, Holographic complexity is nonlocal, J. High Energy Phys. 02 (2018) 072.

[21] R. G. Cai, S. M. Ruan, S. J. Wang, R. Q. Yang, and R. H. Peng, Action growth for AdS black holes, J. High Energy Phys. 09 (2016) 161.

[22] R. Q. Yang and S. M. Ruan, Comments on joint terms in gravitational action, Classical Quantum Gravity **34**, 175017 (2017).

[23] W. D. Guo, S. W. Wei, Y. Y. Li, and Y. X. Liu, Complexity growth rates for AdS black holes in massive gravity and $f(R)$ gravity, Eur. Phys. J. C **77**, 904 (2017).

[24] J. Couch, S. Eccles, T. Jacobson, and P. Nguyen, Holographic complexity and volume, J. High Energy Phys. 11 (2018) 044.

[25] M. Zhang, C. Fang, and J. Jiang, Holographic complexity of rotating black holes with conical deficits, Phys. Lett. B **838**, 137691 (2023).

[26] L. Susskind and Y. Zhao, Switchbacks and the bridge to nowhere, arXiv:1408.2823.

[27] S. Chapman, H. Marrochio, and R. C. Myers, Complexity of formation in holography, J. High Energy Phys. 01 (2017) 062.

[28] R. G. Cai, M. Sasaki, and S. J. Wang, Action growth of charged black holes with a single horizon, Phys. Rev. D **95**, 124002 (2017).

[29] Y. S. An and R. H. Peng, Effect of the dilaton on holographic complexity growth, Phys. Rev. D **97**, 066022 (2018).

[30] K. Goto, H. Marrochio, R. C. Myers, L. Queimada, and B. Yoshida, Holographic complexity equals which action?, J. High Energy Phys. 02 (2019) 160.

[31] A. Bernamonti, F. Galli, J. Hernandez, R. C. Myers, S. M. Ruan, and J. Simón, First law of holographic complexity, Phys. Rev. Lett. **123**, 081601 (2019).

[32] A. Bernamonti, F. Bigazzi, D. Billo, L. Faggi, and F. Galli, Holographic and QFT complexity with angular momentum, J. High Energy Phys. 11 (2021) 037.

[33] A. Belin, R. C. Myers, S. M. Ruan, G. Sárosi, and A. J. Speranza, Does complexity equal anything?, Phys. Rev. Lett. **128**, 081602 (2022).

[34] A. Belin, R. C. Myers, S. M. Ruan, G. Sárosi, and A. J. Speranza, Complexity equals anything II, J. High Energy Phys. 01 (2023) 154.

[35] E. Jørstad, R. C. Myers, and S. M. Ruan, Complexity = Anything: Singularity probes, J. High Energy Phys. 07 (2023) 223.

[36] F. Omidi, Generalized volume-complexity for two-sided hyperscaling violating black branes, J. High Energy Phys. 01 (2023) 105.

[37] M. T. Wang, H. Y. Jiang, and Y. X. Liu, Generalized volume-complexity for RN-AdS black hole, J. High Energy Phys. 07 (2023) 178.

[38] X. Wang, R. Li, and J. Wang, Generalized volume complexity in Gauss-Bonnet gravity: Constraints and phase transitions, Phys. Rev. D **108**, 126018 (2023).

[39] A. Akhavan and F. Omidi, On the role of counterterms in holographic complexity, J. High Energy Phys. 11 (2019) 054.

[40] F. Omidi, Regularizations of action-complexity for a pure BTZ black hole microstate, J. High Energy Phys. 07 (2020) 020.

[41] R. Q. Yang, H. S. Jeong, C. Niu, and K. Y. Kim, Complexity of holographic superconductors, J. High Energy Phys. 04 (2019) 146.

[42] Y. Shi, Q. Pan, and J. Jing, Holographic subregion complexity in unbalanced holographic superconductors, Eur. Phys. J. C **81**, 228 (2021).

[43] Y. S. An, L. Li, F. G. Yang, and R. Q. Yang, Interior structure and complexity growth rate of holographic superconductor from M-theory, J. High Energy Phys. 08 (2022) 133.

[44] S. A. Hartnoll, C. P. Herzog, and G. T. Horowitz, Building a holographic superconductor, Phys. Rev. Lett. **101**, 031601 (2008).

[45] S. A. Hartnoll, G. T. Horowitz, J. Kruthoff, and J. E. Santos, Diving into a holographic superconductor, SciPost Phys. **10**, 009 (2021).

[46] M. Baggioli, K. Y. Kim, L. Li, and W. J. Li, Holographic axion model: A simple gravitational tool for quantum matter, Sci. China Phys. Mech. Astron. **64**, 270001 (2021).

[47] Y. J. He, J. Tian, and B. Chen, Deformed integrable models from holomorphic Chern-Simons theory, Sci. China Phys. Mech. Astron. **65**, 100413 (2022).

[48] L. OuYang, D. Wang, X. Qiao, M. Wang, Q. Pan, and J. Jing, Holographic insulator/superconductor phase transitions with excited states, Sci. China Phys. Mech. Astron. **64**, 240411 (2021).

[49] R. Jefferson and R. C. Myers, Circuit complexity in quantum field theory, J. High Energy Phys. 10 (2017) 107.

[50] L. Hackl and R. C. Myers, Circuit complexity for free fermions, J. High Energy Phys. 07 (2018) 139.

[51] M. Guo, J. Hernandez, R. C. Myers, and S. M. Ruan, Circuit complexity for coherent states, J. High Energy Phys. 10 (2018) 011.

[52] E. Caceres, S. Chapman, J. D. Couch, J. P. Hernandez, R. C. Myers, and S. M. Ruan, Complexity of mixed states in QFT and holography, J. High Energy Phys. 03 (2020) 012.

[53] S. M. Ruan, Purification complexity without purifications, J. High Energy Phys. 01 (**2021**) 092.

[54] T. Anegawa, N. Iizuka, and M. Nishida, Krylov complexity as an order parameter for deconfinement phase transitions at large N, J. High Energy Phys. 04 (2024) 119.

[55] D. E. Parker, X. Cao, A. Avdoshkin, T. Scaffidi, and E. Altman, A universal operator growth hypothesis, Phys. Rev. X **9**, 041017 (2019).

[56] P. Caputa, J. M. Magan, and D. Patramanis, Geometry of Krylov complexity, Phys. Rev. Res. **4**, 013041 (2022).

[57] A. Dymarsky and M. Smolkin, Krylov complexity in conformal field theory, Phys. Rev. D **104**, L081702 (2021).

[58] A. Avdoshkin, A. Dymarsky, and M. Smolkin, Krylov complexity in quantum field theory, and beyond, J. High Energy Phys. 06 (2024) 066.

[59] B. Bhattacharjee, X. Cao, P. Nandy, and T. Pathak, Krylov complexity in saddle-dominated scrambling, J. High Energy Phys. 05 (2022) 174.

[60] F. B. Trigueros and C. J. Lin, Krylov complexity of many-body localization: Operator localization in Krylov basis, SciPost Phys. **13**, 037 (2022).

[61] H. A. Camargo, V. Jahnke, K. Y. Kim, and M. Nishida, Krylov complexity in free and interacting scalar field theories with bounded power spectrum, J. High Energy Phys. 05 (2023) 226.

[62] A. Reynolds and S. F. Ross, Complexity in de Sitter space, Classical Quantum Gravity **34**, 175013 (2017).

[63] E. Jørstad, R. C. Myers, and S. M. Ruan, Holographic complexity in dS$_{d+1}$, J. High Energy Phys. 05 (2022) 119.

[64] P. Caputa and S. Liu, Quantum complexity and topological phases of matter, Phys. Rev. B **106**, 195125 (2022).

[65] R. Suzuki, J. Haferkamp, J. Eisert, and P. Faist, Quantum complexity phase transitions in monitored random circuits, arXiv:2305.15475.

[66] S. Roca-Jerat, T. Sancho-Lorente, J. Román-Roche, and D. Zueco, Circuit complexity through phase transitions: Consequences in quantum state preparation, SciPost Phys. **15**, 186 (2023).

[67] J. Yang and A. R. Frey, Complexity, scaling, and a phase transition, J. High Energy Phys. 09 (2023) 029.

[68] R. Auzzi, G. Nardelli, G. P. Ungureanu, and N. Zenoni, Volume complexity of dS bubbles, Phys. Rev. D **108**, 026006 (2023).

[69] Y. Wang and J. Ren, Holographic complexity of hyperbolic black holes, Phys. Rev. D **108**, 046006 (2023).

[70] R. G. Cai, Gauss-Bonnet black holes in AdS spaces, Phys. Rev. D **65**, 084014 (2002).

[71] M. Banados, C. Teitelboim, and J. Zanelli, The black hole in three-dimensional space-time, Phys. Rev. Lett. **69**, 1849 (1992).

[72] C. Martinez, C. Teitelboim, and J. Zanelli, Charged rotating black hole in three space-time dimensions, Phys. Rev. D **61**, 104013 (2000).

[73] H. A. Camargo, V. Jahnke, H. S. Jeong, K. Y. Kim, and M. Nishida, Spectral and Krylov complexity in billiard systems, Phys. Rev. D **109**, 046017 (2024).